Research Article | Vol. 31, No. 15 / 17 Jul 2023 / Optics Express 23889
Optics EXPRESS

In-situ analysis of combustion aerosol using a supercontinuum lidar

ABBA SALEH,* KIM KALMANKOSKI, GOËRY GENTY, AND JUHA TOIVONEN

Photonics Laboratory, Physics Unit, Tampere University, P.O. Box 692, FI-33101 Tampere, Finland
**abba.saleh@tuni.fi*

Abstract: We report real-time monitoring of coarse aerosol particle distribution in a 9 m wide full-scale industrial boiler using a broadband supercontinuum lidar. The technique utilizes the light backscattered from the aerosol to map the extinction profile using the Klett inversion method, with measured extinction values of $0.04 - 0.2\,\mathrm{m}^{-1}$ across the furnace. The technique further exploits differential absorption of water molecules in the $1.25 - 1.5\,\mu\mathrm{m}$ region to map the water vapor concentration profile in the furnace up to a distance of 3.9 m with a spatial resolution of 30 cm. We also take advantage of the strong reflection from the boiler back-wall to simultaneously measure the average water vapor temperature and concentration in the boiler in good agreement with reference readings from the boiler. Our results open novel perspectives for versatile 3D profiling of flue gas parameters and other industrial process analysis.

1. Introduction

Owing to its CO_2 neutrality, biomass has gained significant attention as an alternative sustainable source of energy and it is nowadays widely used as renewable fuel in combustion power plant boilers. However, the exact composition of biomass can vary significantly such that optimal performance of the combustion process generally requires dynamic monitoring of the flue gas parameters, including temperature, molecular concentrations and fly ash aerosol particles. Aerosol particles can further act as contaminants which may cause malfunction in the combustion unit. For example, alkali chloride salt particles, such as KCl and CaCl, naturally produced during the combustion process can deposit on the surface of heat exchangers or other critical components of the combustion unit, and their reaction with these surfaces often leads to corrosion [1–3] and fouling [4–6]. This in turn can critically affect the convective heat transfer essential for the combustion process. Additionally, the aerosol size distribution and concentration can yield important information regarding the boiler bed conditions [7] as well as the fuel quality [8].

The conventional approach to monitor combustion aerosols relies on extracting the aerosol particles from the combustion unit via a suction tube to a designated measurement device [9,10]. A similar technique is also used to measure the molecular concentration of probed gases [11,12]. This approach however poses significant challenges such as latency, condensation in the tubes and possible nucleation or coagulation of the particles, complicating real-time probing of the flue gas parameters. Alternative methods based on optical spectroscopy [13–17] have been introduced for gas-phase reaction studies in combustion applications, but they require at least two openings on the furnace walls as they measure the transmitted signal through a particular area. This makes their application to combustion units with limited openings, such as boilers, unpractical. Techniques based on light detection and ranging (lidar) that are based on reflected light do not require multiple opening and are particularly adapted to remote measurement of flue gas parameters [18–20]. These techniques however are limited to probing one flue gas component at a time. Recently, we have introduced a new lidar system employing a broadband

#492715 https://doi.org/10.1364/OE.492715
Journal © 2023 Received 12 Apr 2023; revised 9 Jun 2023; accepted 13 Jun 2023; published 5 Jul 2023

Optics EXPRESS

supercontinuum light source capable of simultaneously probing the flue gas temperature and molecular concentration in an industrial boiler [21,22].

Herein, we expand this recent work and demonstrate a supercontinuum lidar (SC-lidar) system capable of simultaneously monitoring the spatially-resolved aerosol particle distribution and measuring the water vapor (H_2O) temperature and concentration in an industrial power plant boiler via a single measurement port. The technique exploits differential absorption between three specific spectral channels in the SC spectrum (Ch1, Ch2 and Ch3 in Fig. 1). Specifically, we map the coarse aerosol particle distribution along the beam path from the signal backscattered by the aerosol particles at SC wavelengths not absorbed in the boiler, and we characterize the water vapor concentration distribution in the furnace up to a distance of 3.9 m by exploiting differential absorption in the SC spectrum. Finally, the average water vapor temperature and concentration in the boiler are obtained from the strong backscattered light from the back-wall of the boiler. Our results highlights the unique potential of the SC-lidar for real-time versatile sensing and process analysis in industrial environments.

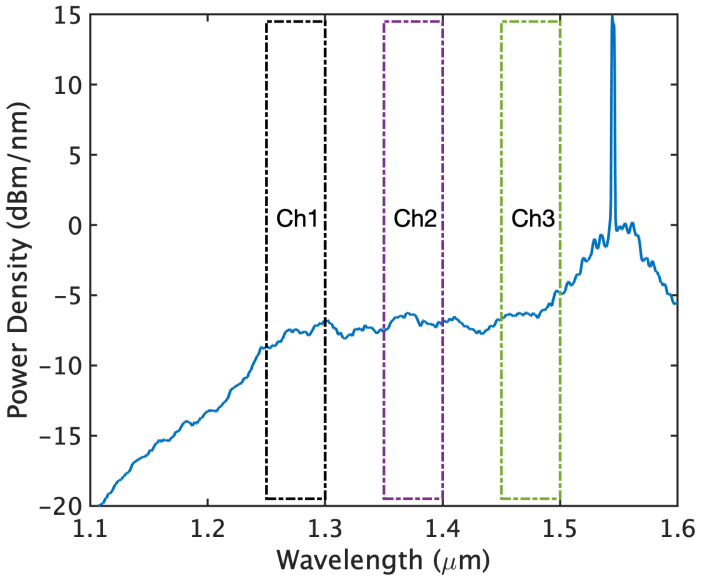

Fig. 1. Power spectral density of the supercontinuum light source with the corresponding full width at half maximum of the SC-lidar spectral channels indicated by the rectangles.

2. Aerosol extinction estimation

The measured extinction coefficient α of a lidar beam generally depends both on the absorption by gaseous species α_{abs} and scattering by aerosol particles α_{sca}, such that $\alpha = \alpha_{abs} + \alpha_{sca}$. The aerosol extinction is generally wavelength dependent especially in Rayleigh and Mie regime. However, considering homogeneous composition of aerosols dominated by coarse particles in the furnace and relatively narrow band of the SC-lidar spectral channels, α_{sca} is mainly proportional to the particle volume fraction on the beam path. In order to obtain the extinction coefficient from a measurement, we begin by including the α_{sca} into the known lidar equation for broad band SC source [22]:

$$S_n(R) = \beta(R)\frac{O(R)}{R^2}\int_{\Delta\lambda_n} P_0(\lambda)\Gamma_n(\lambda)e^{-2\int_0^R \alpha_{abs}(\lambda,T,R') + \alpha_{sca}(R')\,dR'}\,d\lambda, \tag{1}$$

Optics EXPRESS

where n denotes the spectral channel and R is the measurement distance. The detected signal is proportional to the aerosol backscattering coefficient $\beta(R)$ and $O(R)$ is the geometrical form factor accounting for the fraction of backscattered signal from a distance R which is effectively detected. $P_0(\lambda)$ is the power spectrum of the SC light source and $\Gamma_n(\lambda)$ is the filter transmission for a given channel n. The absorption effect on extinction can be neglected for spectral channels which are outside the absorption wavelength range (Ch1 in our case). Therefore, Eq. (1) reduces to

$$S_1(R) = \beta(R)\frac{O(R)}{R^2}P_1 e^{-2\int_0^R \alpha(R')\,dR'}, \tag{2}$$

where $P_1 = \int_{\Delta\lambda_n} P_0(\lambda)\Gamma_1(\lambda)\,d\lambda$. Note that for a homogeneous aerosol mixture $\beta = L\alpha$ [23], where L is the ratio of aerosol specific backscattering coefficient to the extinction coefficient. Eq. (2) is analogous to the typical elastic backscatter lidar equation, thus, the aerosol distribution in the furnace can be estimated by solving for the extinction coefficient using the inversion method introduced by Klett [23,24]. The method is widely used in atmospheric lidar applications due to its stability and tolerance to noise [25]. The method involves estimating the extinction coefficient in a reference distance using

$$\alpha(R) = \frac{e^{W(R)-W(R_m)}}{\frac{1}{\alpha(R_m)} + 2\int_R^{R_m} e^{W(R')-W(R_m)}\,dR'}, \tag{3}$$

where W is a logarithmic range corrected signal ($ln[\frac{S_1(R)R^2}{O(R)}]$), R_m is a chosen reference distance such that $R<R_m$. One can also estimate the initial values of extinction at a given reference distance by a simple slope method suggested by Klett as $\alpha(R_m) = \frac{1}{2}\frac{W_0-W_m}{R_m-R_0}$, where the zero subscript denotes the starting point of the slope. This means that knowing the aerosol backscattered signal Ch1, the geometrical form factor and the measurement distance is sufficient to estimate the extinction coefficient.

3. Experiment

The supercontinuum is generated by injecting sub-nanosecond pulses at 1547 nm from a gain-switched fiber laser (Keopsys-PEFL-K09) producing 10 kW peak power at 100 kHz repetition rate into the anomalous dispersion regime of a 30-cm-long silica dispersion-shifted fiber (DSF, Corning, Inc. LEAF) with zero dispersion wavelength (ZDW) at 1510 nm followed by a 3-m-long dispersion compensating fiber (DCF4, Thorlabs) with ZDW at 1583 nm. The 1510 nm zero dispersion wavelength (ZDW) of the DSF enables noise-seeded modulation instability, breaking up the long pump pulses into a large number of solitons. Subsequent propagation in the dispersion compensating fiber allows for soliton dynamics for wavelengths above 1583 nm (including dispersive wave generation, Raman self-frequency shift and cross-phase modulation) yielding efficient energy transfer in the 1.1-1.6 microns region. The resulting SC spectrum covers 0.8 – 2.4 µm up to the silica transparency window. The output SC pulses have the same pulse parameters as the input pump pulses. Fig. 1 shows the SC power spectral density in the 1.1 – 1.6 µm spectral range of interest for our experiments. The full width at half maximum (FWHM) of the bandpass filters used as spectral channels for the lidar measurements are also marked in the figure.

The lidar measurements were conducted in a 9-m-wide bubbling fluidized bed (BFB) biomass boiler with thermal power of 190 MW. A schematic illustration of the experimental setup is shown in the inset in Fig. 2. The setup is similar to that in Ref. 22 except for the bandpass filters associated with the three spectral channels, which are different (87-852, 87-867 & 87-856, Edmund Optics) and are specifically selected to ensure optimal coverage of the differently absorbing spectral channels. The setup also includes a field programmable gate array (FPGA) board (EK-U1-ZCU111-G, Xlinx) which utilizes the built-in 12-bit analog-to-digital converter

Optics EXPRESS

to digitize the signals after the amplifier at a sampling rate of 4 GHz. This process is repeated iteratively averaging up to 3 x 10^5 signals per individual channel over a total measurement time of 3 s. Constant measurement time and averaging was used in all measurements. Figure 2 shows an example of recorded signal where we can identify three distinct peaks at different delay times. The first peak near −10 ns represents scattering from the coupling mirror placed in front of the receiver optics. The backscattered signal from the aerosol particles corresponds to the broad skewed peak starting at 0 ns and the peak around 60 ns originates from the boiler back-wall reflection.

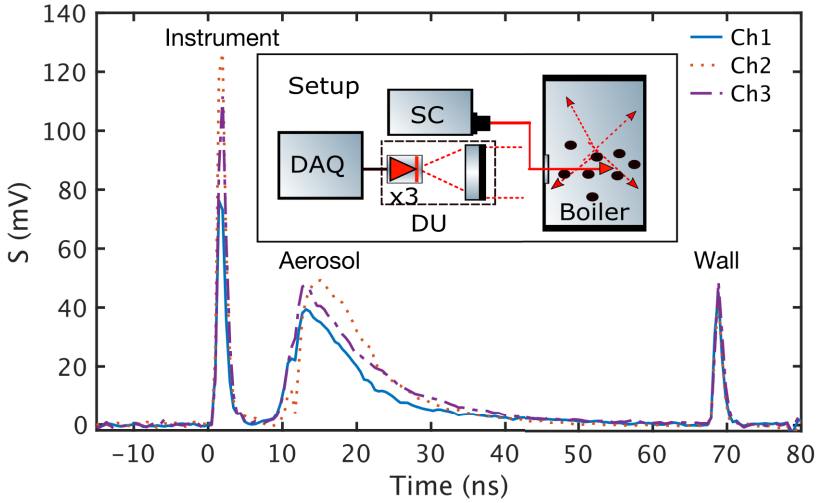

Fig. 2. Measured SC-lidar signal from a full-scale industrial boiler. Ch1 (solid line), Ch2 (dotted line) and Ch3 (dashed line) represents the signal from the three specific spectral channels used in the supercontinuum spectrum. Inset is the corresponding experimental setup. DU: detection unit, DAQ: data acquisition.

4. Results

The aerosol distribution in the furnace can be retrieved from the Ch1 backscattered signal, which corresponds to the spectral channel with negligible absorbance in the beam path, where the extinction in the lidar beam is mainly due to scattering by the aerosol particles. The geometrical form factor $O(R)$ is evaluated by continuously displacing a diffusing hard target over a given distance R, and measuring the backscattered signal multiple times. The measurement was done outside of the boiler furnace to exclude aerosol extinction effect inside the boiler. A polynomial piece-wise fitting is applied to obtain a continuous form factor function that applies to all data points. The form factor and measurement distance are used to cancel out the geometrical effect on the signal. Figure 3 shows the range corrected signal (solid blue line) and the corresponding geometrical form factor of our SC-lidar system (dashed red line). The initial values for extinction are calculated using $R_0 = 1\,m$ and $R_m = 8\,m$, representing an interval with adequate signal-to-noise ratio (SNR) and a clear slope in the logarithmic range corrected signal W. The extinction values are extracted using the resulting initial values in Eq. (3), and the corresponding extinction map is shown in the lower panel in Fig. 4. It represents a 90 s extinction time series across the furnace. The 90 s time window is arbitrarily selected with respect to the furnace operational timeline. The resulting extinction values imply a dynamic concentration distribution of the aerosol particles. The extinction values at 1 – 2 m distance in the furnace slightly fluctuates around 0.1 m^{-1} over time, with a standard deviation of 0.01m^{-1}, corresponding to a relatively

Optics EXPRESS

moderate concentration of the aerosol particles. The variation in the extinction values (i.e. the distribution of the aerosol particles concentration) becomes more pronounced at longer distances, with extinction values in the range of $0.04 - 0.2\,\mathrm{m}^{-1}$. The inhomogeneous aerosol concentration distribution in the furnace can be attributed to the air feed for the combustion process, due to the correlation between air flow and particle distribution. This in turn could be exploited to complement flow measurements in the furnace. Further analysis of the aerosol concentration distribution can also yield information regarding the fuel quality [8]. Finally, optimizing the SC-lidar to enable particle size distribution analysis would pave the way for monitoring the boiler bed conditions [7]. This can be achieved using multi-octave spanning broadband light sources.

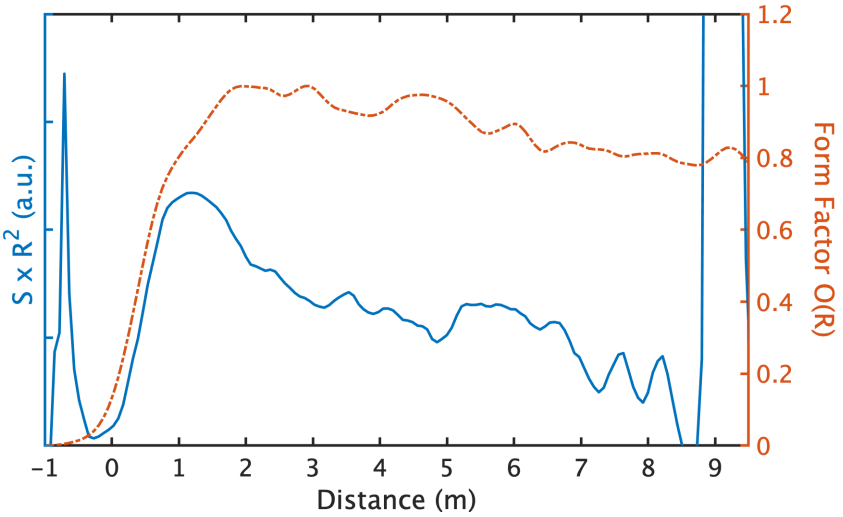

Fig. 3. Measured Ch1 range corrected signal (solid line) and the corresponding geometrical form factor of the SC-lidar (dashed line). The bang in the corrected signal at around 9 m originates from the boiler back wall reflection.

Analysis of temperature and molecular concentrations also plays a central role in the optimization of the combustion processes as aforementioned in the introduction section. To map out temperature and molecular concentrations in the furnace, one can further utilize the backscattered signal from the aerosol particles in spectral channels corresponding to the absorption region of H_2O (which is one of the primary flue gas component with rich absorption spectrum in the infrared). Specifically, variations in H_2O concentration were obtained from the backscattered signal from the aerosol particles in spectral channels Ch1 and Ch2 and using a reference temperature value of 850 °C in Eq. 3 of Ref. 22. The H_2O concentration profile along the beam path could be resolved up to a distance of 3.9 m as shown in Fig. 5, limited by the SNR of our measurement. The SNR also restricts mapping of temperature variation in the furnace, as the temperature induced relative change in the backscattered signal intensity is comparable to the noise amplitude of the recorded data. In this respect, the detector, amplifier and FPGA associated readout noise as well as the supercontinuum source spectral instabilities are currently the main sources of noise in this experiment. In order to enhance the SNR and increase the probing distance of our lidar system, there are several improvements which could be implemented. These include increasing the continuous averaging during the detection, using a detector with better noise performance, or using a supercontinuum with higher power spectral density and lower relative intensity noise.

Nonetheless, one can also exploit the strong instrument and back-wall reflection in the SC-lidar signal in Fig. 2 to extract both the average H_2O temperature and concentration in the furnace

Optics EXPRESS

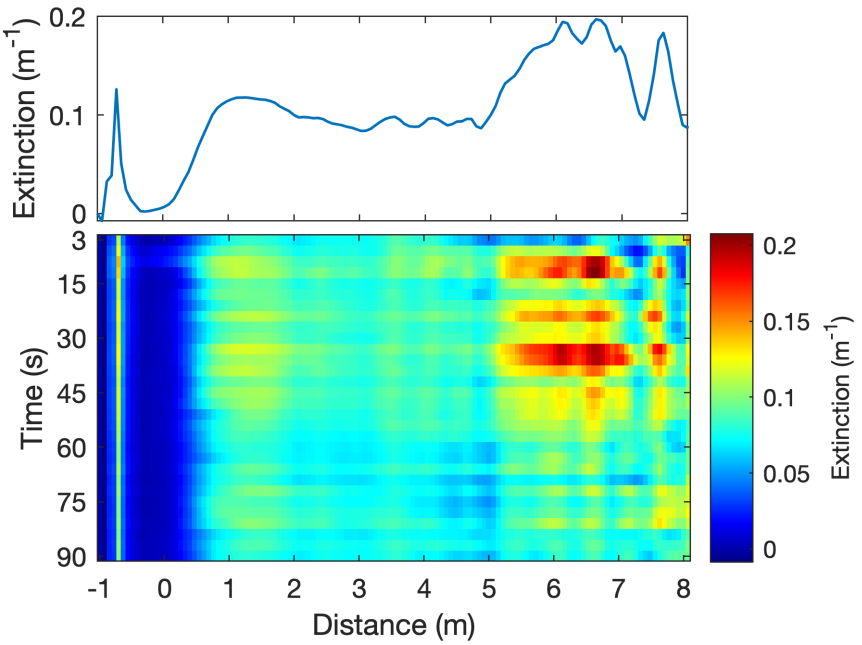

Fig. 4. Bottom panel: measured extinction profile of the coarse aerosol particles in the boiler over 30 consecutive measurements with a corresponding total measurement time of 90 s. Top panel: an example of a single measurement from the time series extinction map.

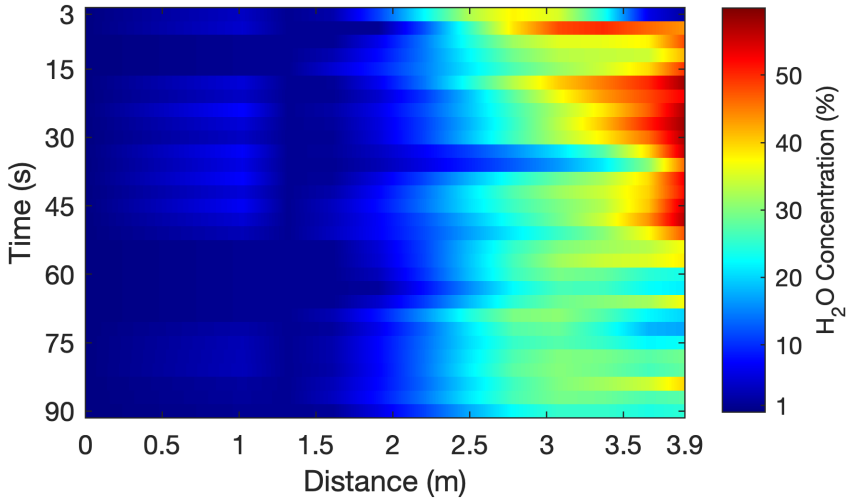

Fig. 5. Measured water vapor concentration variation in the boiler over 30 consecutive measurements with a corresponding total measurement time of 90 s.

by simultaneously solving for Eq. (3) and Eq. (4) of Ref. 22. This yields values of 830 °C and 20.6 % for average H_2O temperature and concentration, respectively, in very good agreement with the reference temperature value of 850 °C (measured with a K-type thermocouple) and concentration in the range 20 – 25 % (estimated based on heat and mass balance calculations [26]). It is also important to emphasize that the results are consistent with earlier reported values [22] appropriate for industrial process analysis.

Optics EXPRESS

5. Conclusion

We have reported proof-of-concept demonstration of in-situ combustion diagnostics in a full-scale industrial boiler using a broadband supercontinuum lidar system via a single optical access. The technique utilizes three specific wavelength bands in the supercontinuum spectrum, which enables versatile analysis of flue gas parameters. With this approach, we have demonstrated spatially-resolved remote measurement of coarse aerosol particle distribution in the boiler, with extinction values in the range of $0.04-0.2\,\mathrm{m}^{-1}$. Our result can be used to complement flow measurements in the furnace due to the correlation between air flow and particle distribution. Average water vapor temperature and concentration in the furnace is also measured with accuracy consistent with earlier reported values [22] and appropriate for industrial process monitoring. We also mapped the water vapor concentration profile up to 3.9 m distance inside the boiler, limited by the signal-to-noise ratio (SNR) of our detection system. A higher SNR would enhance the probing distance and in principle enable spatially resolving the gas temperature. In the future, we believe that supercontinuum-based lidar systems can be further expanded to perform full 3D mapping of flue gas parameters in combustion environments and other versatile industrial process monitoring, by steering the incident probe beam using a special mirror arrangement or other advanced micro-electro-mechanical systems (MEMS).

Funding. Academy of Finland (320165).

Acknowledgments. A.S acknowledges the support from Finnish Foundation for Technology Promotion. The authors are sincerely grateful to Jaani Silvennoinen and Jari Perälä for organizing the measurement campapaign, and Tampereen Sähkölaitos for making their power plant accessible and the hospitality.

Disclosures. The authors declare no conflicts of interest.

Data availability. Data underlying the results presented in this paper are not publicly available at this time but may be obtained from the authors upon reasonable request.

References

1. R. A. Antunes and M. C. L. de Oliveira, "Corrosion in biomass combustion: A materials selection analysis and its interaction with corrosion mechanisms and mitigation strategies," Corros. Sci. **76**, 6–26 (2013).
2. H. P. Nielsen, F. Frandsen, K. Dam-Johansen, and L. Baxter, "The implications of chlorine-associated corrosion on the operation of biomass-fired boilers," Prog. Energy Combust. Sci. **26**(3), 283–298 (2000).
3. E. Vainio, N. DeMartini, L. Hupa, L.-E. Åmand, T. Richards, and M. Hupa, "Hygroscopic properties of calcium chloride and its role on cold-end corrosion in biomass combustion," Energy Fuels **33**(11), 11913–11922 (2019).
4. M. Theis, B.-J. Skrifvars, M. Hupa, and H. Tran, "Fouling tendency of ash resulting from burning mixtures of biofuels. part 1: Deposition rates," Fuel **85**(7-8), 1125–1130 (2006).
5. B.-J. Skrifvars, P. Yrjas, T. Laurén, J. Kinni, H. Tran, and M. Hupa, "The fouling behavior of rice husk ash in fluidized-bed combustion. 2. pilot-scale and full-scale measurements," Energy Fuels **19**(4), 1512–1519 (2005).
6. A. F. Stam, K. Haasnoot, and G. Brem, "Superheater fouling in a bfb boiler firing wood-based fuel blends," Fuel **135**, 322–331 (2014).
7. B.-Å. Andersson, "Effects of bed particle size on heat transfer in circulating fluidized bed boilers," Powder Technol. **87**(3), 239–248 (1996).
8. A. Garcia-Maraver, M. Zamorano, U. Fernandes, M. Rabaçal, and M. Costa, "Relationship between fuel quality and gaseous and particulate matter emissions in a domestic pellet-fired boiler," Fuel **119**, 141–152 (2014).
9. E. Gustafsson, L. Lin, M. C. Seemann, J. Rodin, and M. Strand, "Characterization of particulate matter in the hot product gas from indirect steam bubbling fluidized bed gasification of wood pellets," Energy Fuels **25**(4), 1781–1789 (2011).
10. H. Kuuluvainen, P. Karjalainen, C. J. Bajamundi, J. Maunula, P. Vainikka, J. Roppo, J. Keskinen, and T. Rönkkö, "Physical properties of aerosol particles measured from a bubbling fluidized bed boiler," Fuel **139**, 144–153 (2015).
11. E. Vainio, A. Brink, M. Hupa, H. Vesala, and T. Kajolinna, "Fate of fuel nitrogen in the furnace of an industrial bubbling fluidized bed boiler during combustion of biomass fuel mixtures," Energy Fuels **26**(1), 94–101 (2012).
12. E. Vainio, *Fate of fuel-bound nitrogen and sulfur in biomass-fired industrial boilers* (Åbo Akademi University, PhD thesis, 2014).
13. T. Sorvajärvi, N. DeMartini, J. Rossi, and J. Toivonen, "In situ measurement technique for simultaneous detection of k, kcl, and koh vapors released during combustion of solid biomass fuel in a single particle reactor," Appl. Spectrosc. **68**(2), 179–184 (2014).
14. X. Zhou, J. Jeffries, and R. Hanson, "Development of a fast temperature sensor for combustion gases using a single tunable diode laser," Appl. Phys. B **81**(5), 711–722 (2005).

Optics EXPRESS

15. M. Aldén, A. Omrane, M. Richter, and G. Särner, "Thermographic phosphors for thermometry: a survey of combustion applications," Prog. Energy Combust. Sci. **37**(4), 422–461 (2011).
16. J. Borggren, W. Weng, A. Hosseinnia, P.-E. Bengtsson, M. Aldén, and Z. Li, "Diode laser-based thermometry using two-line atomic fluorescence of indium and gallium," Appl. Phys. B **123**(12), 278 (2017).
17. J. Viljanen, T. Sorvajärvi, and J. Toivonen, "In situ laser measurement of oxygen concentration and flue gas temperature utilizing chemical reaction kinetics," Opt. Lett. **42**(23), 4925–4928 (2017).
18. B. Kaldvee, J. Bood, and M. Aldén, "Picosecond-lidar thermometry in a measurement volume surrounded by highly scattering media," Meas. Sci. Technol. **22**(12), 125302 (2011).
19. E. Malmqvist, J. Borggren, M. Aldén, and J. Bood, "Lidar thermometry using two-line atomic fluorescence," Appl. Opt. **58**(4), 1128–1133 (2019).
20. E. Malmqvist, M. Brydegaard, M. Aldén, and J. Bood, "Scheimpflug lidar for combustion diagnostics," Opt. Express **26**(12), 14842–14858 (2018).
21. A. Saleh, A. Aalto, P. Ryczkowski, G. Genty, and J. Toivonen, "Short-range supercontinuum-based lidar for temperature profiling," Opt. Lett. **44**(17), 4223–4226 (2019).
22. A. Saleh, P. Ryczkowski, G. Genty, and J. Toivonen, "Supercontinuum lidar for industrial process analysis," Opt. Express **29**(25), 42082–42089 (2021).
23. J. D. Klett, "Lidar inversion with variable backscatter/extinction ratios," Appl. Opt. **24**(11), 1638 (1985).
24. J. D. Klett, "Stable analytical inversion solution for processing lidar returns," Appl. Opt. **20**(2), 211 (1981).
25. A. Comerón, C. Mu noz-Porcar, F. Rocadenbosch, A. Rodríguez-Gómez, and M. Sicard, "Current Research in Lidar Technology Used for the Remote Sensing of Atmospheric Aerosols," Sensors **17**(6), 1450 (2017).
26. K. C. Weston, "Energy conversion. chapter 3: Fuels and combustion," (1992).